# Cerium-doped $CoMn_2O_4$ Spinels as Highly Efficient Bifunctional Electrocatalysts for ORR/OER Reactions

## Supporting information

**Xiao Chen[1,2], Fengshuang Han[1], Xi Chen[1], Chenxi Zhang[1], and Wangyan Gou [2,*]**

[1] School of Materials Science and Engineering, North China University of Water Resources and Electric Power, Zhengzhou 450045, China;
[2] Key Laboratory of Special Functional and Smart Polymer Materials of Ministry of Industry and Information Technology, School of Chemistry and Chemical Engineering, Northwestern Polytechnical University, Xi'an 710072, China;
* Correspondence: gouwangyan@nwpu.edu.cn

**Table S1.** The ICP results of Ce-CMO-X

| Sample | Solution for ICP-MS (mL) | Measured Ce concentration (ppm) | Mass weight of Ce (wt%) |
|---|---|---|---|
| Ce-CMO-14% | 4 | 175 | 14 |
| Ce-CMO-18% | 4 | 225 | 18 |
| Ce-CMO-22% | 4 | 275 | 22 |

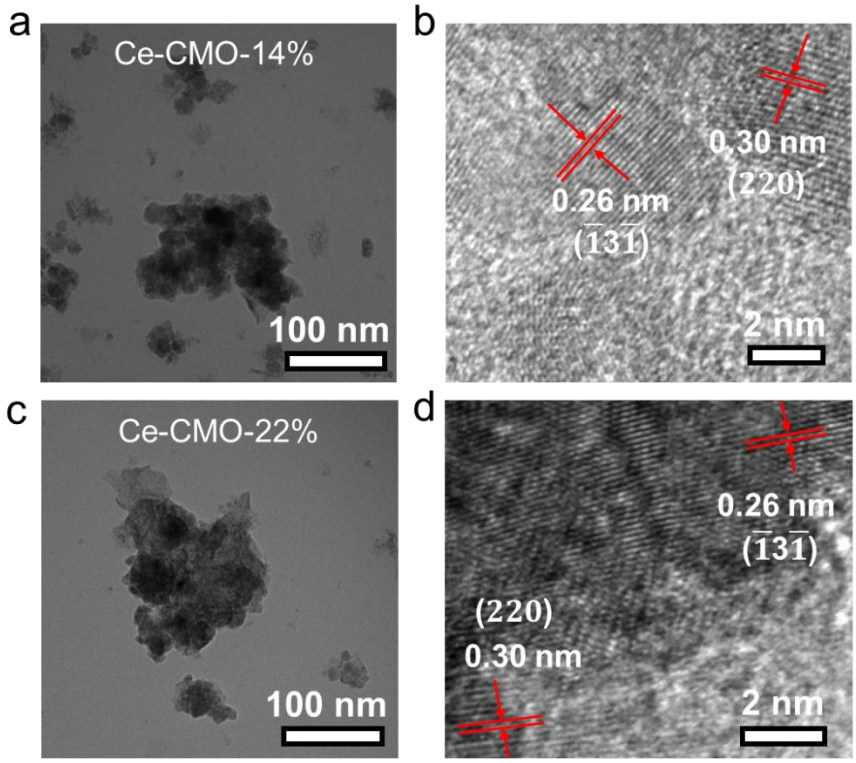


**Figure S1.** The characterization of catalysts: (a) TEM image and (b) HRTEM image of Ce-CMO-14% nanoparticles; (c) TEM image and (d) HRTEM image of Ce-CMO-22% nanoparticles.

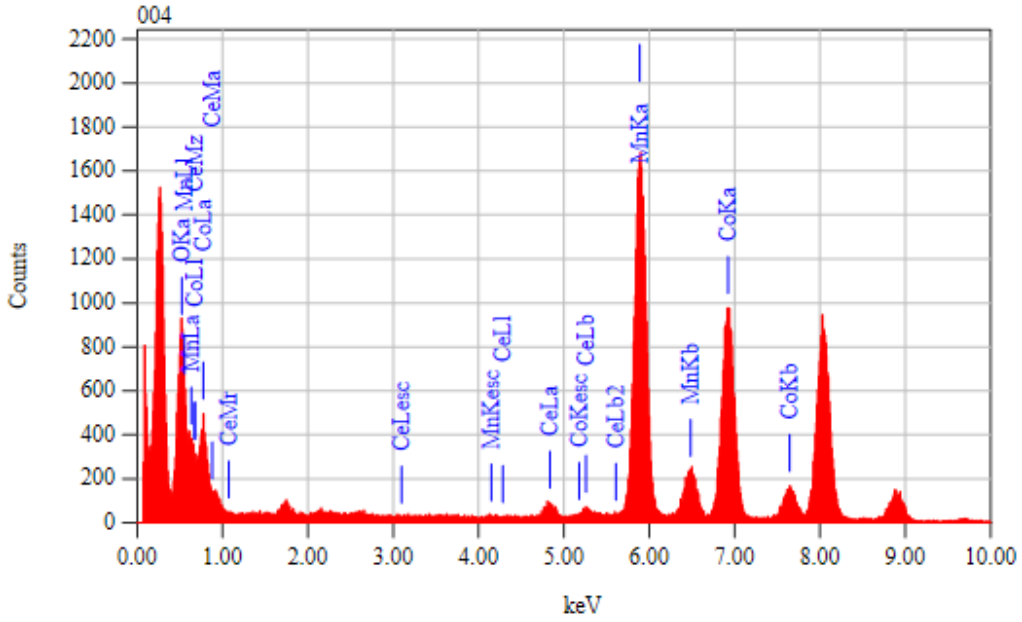


**Figure S2.** The existence of Co, Mn, and Ce elements in Ce-CMO-18% according to EDS mapping.

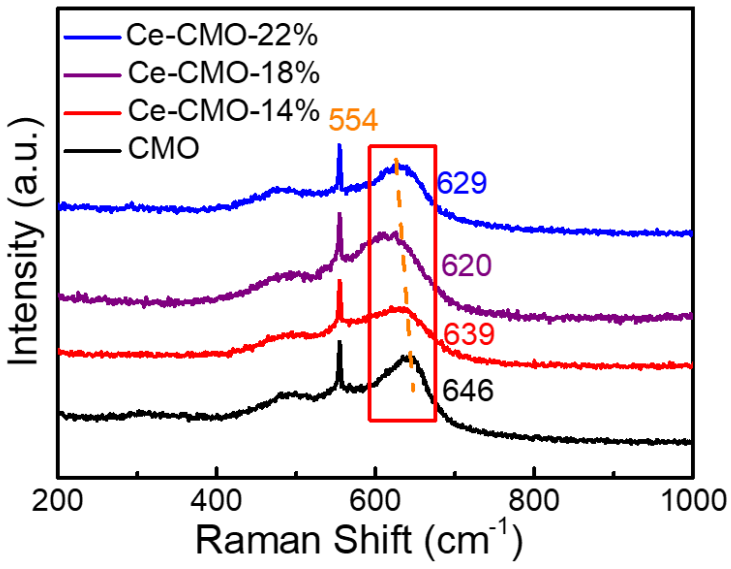


**Figure S3.** The Raman spectrum of pristine CMO, Ce-CMO-14%, Ce-CMO-18%, and Ce-CMO-22%.

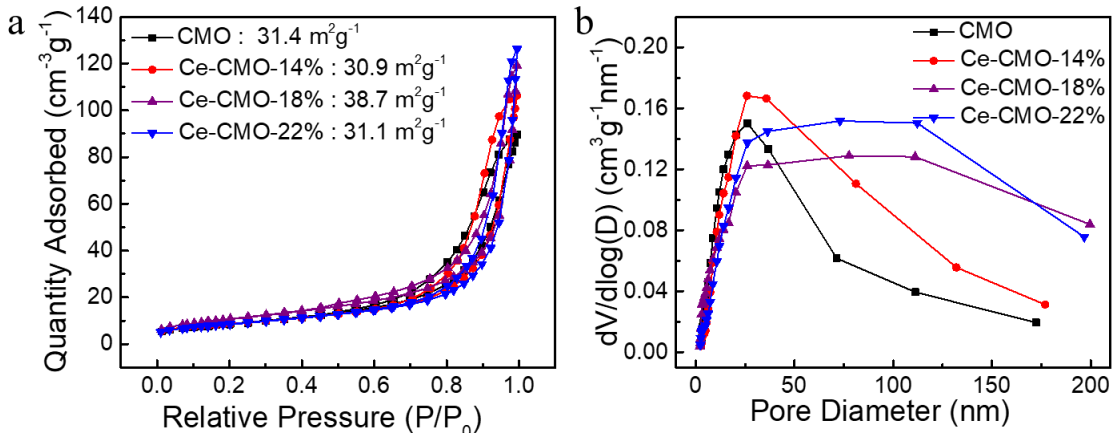


**Figure S4.** (a) $N_2$ adsorption-desorption isotherms and (b) pore diameter distributions of pristine CMO, Ce-CMO-14%, Ce-CMO-18%, and Ce-CMO-22%.

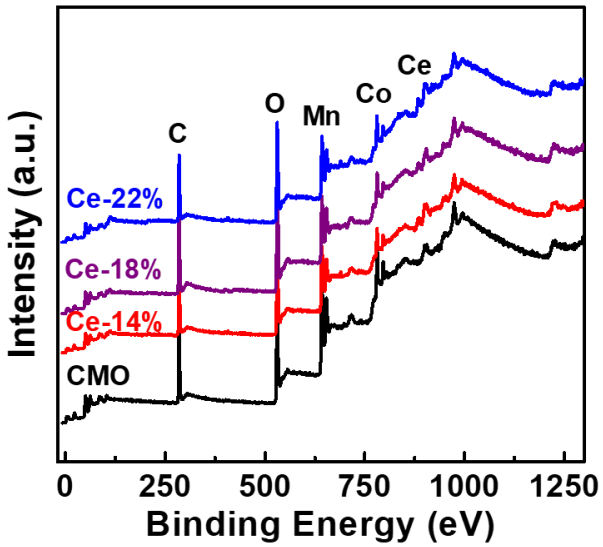


**Figure S5.** The elemental survey of XPS of pristine CMO, Ce-CMO-14%, Ce-CMO-18%, and Ce-CMO-22%.

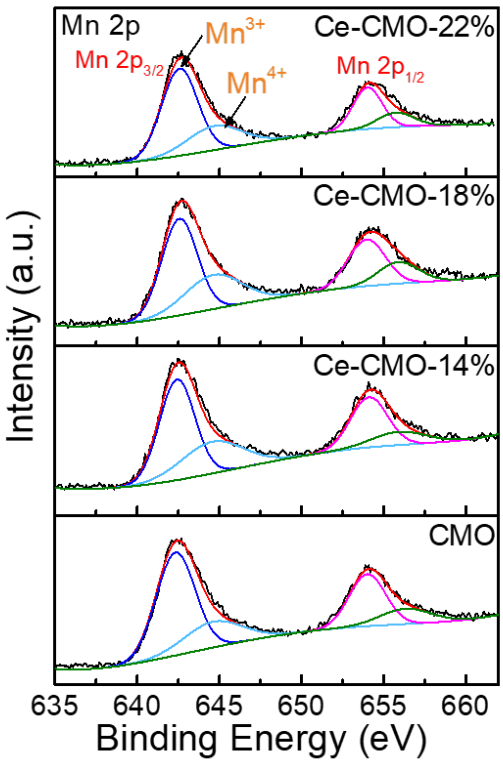


**Figure S6.** The Mn 2p spectra of pristine CMO, Ce-CMO-14%, Ce-CMO-18%, and Ce-CMO-22%.

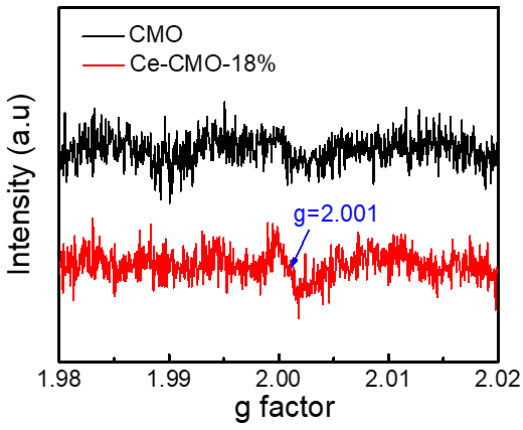


**Figure S7.** The EPR spectra of CMO and Ce-CMO-18%.

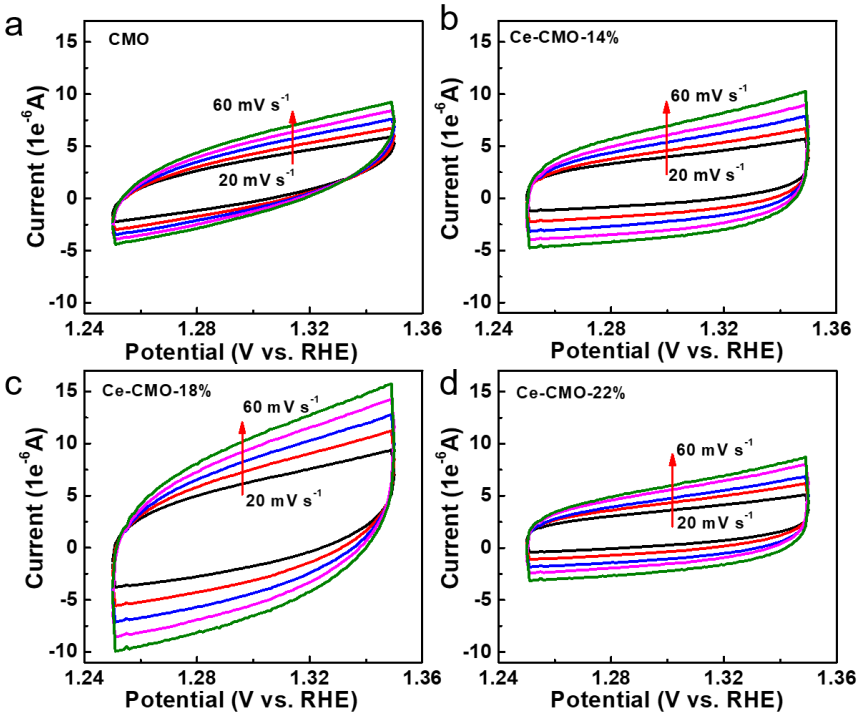


**Figure S8.** The cyclic voltammograms of (a) pristine CMO, (b) Ce-CMO-14%, (c) Ce-CMO-18%, and (d) Ce-CMO-22% at various scan rates (20-60 mV $s^{-1}$).

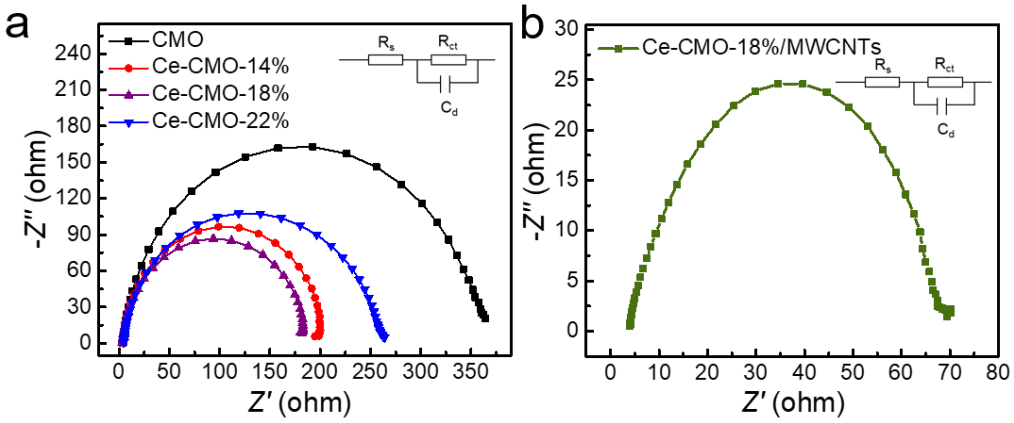


**Figure S9.** The Nyquist diagrams of (a) CMO, Ce-CMO-14%, Ce-CMO-18%, Ce-CMO-22%, and (b) Ce-CMO-18%/MWCNTs.

**Table S2.** The EIS results of CMO, Ce-CMO-X, And Ce-CMO-18%/MWCNTs

| Samples | $R_s$ (Ω) | n | $R_{ct}$ (Ω) | $C_\varphi$ (mF) |
|---|---|---|---|---|
| CMO | 3.45 | 0.92 | 362.6 | 0.135 |
| Ce-CMO-14% | 3.35 | 0.94 | 207.0 | 0.069 |
| Ce-CMO-18% | 325 | 0.93 | 190.2 | 0.118 |
| Ce-CMO-22% | 4.32 | 0.91 | 253.4 | 0.054 |
| Ce-CMO-18%/MWCNTs | 3.78 | 0.78 | 66.8 | 0.262 |

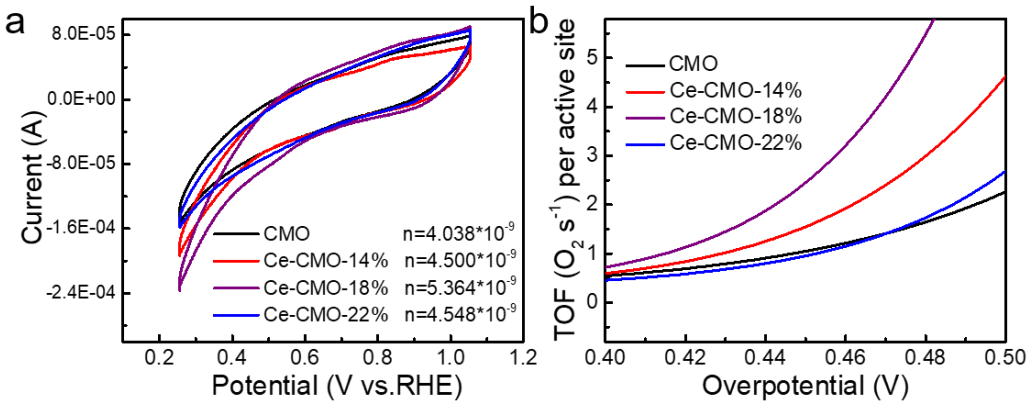


**Figure S10.** (a) CV curves of CMO, Ce-CMO-14%, Ce-CMO-18%, and Ce-CMO-22%, in PBS solution (pH=7.0) at a scan rate of 50 mV $s^{-1}$, (b) Calculated $O_2$ TOF values of CMO, Ce-CMO-14%, Ce-CMO-18%, and Ce-CMO-22%.

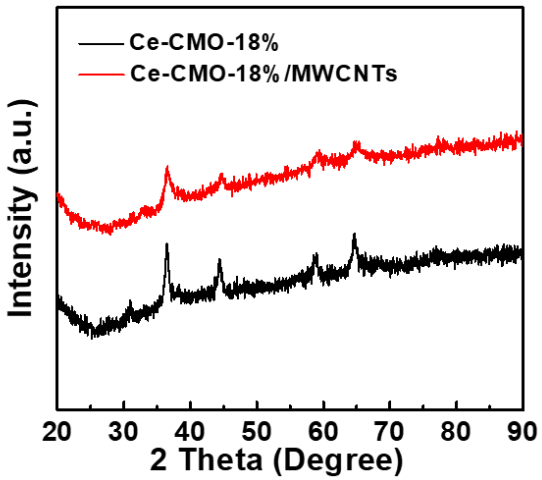


**Figure S11.** The XRD patterns of Ce-CMO-18% and Ce-CMO-18%/MWCNTs.

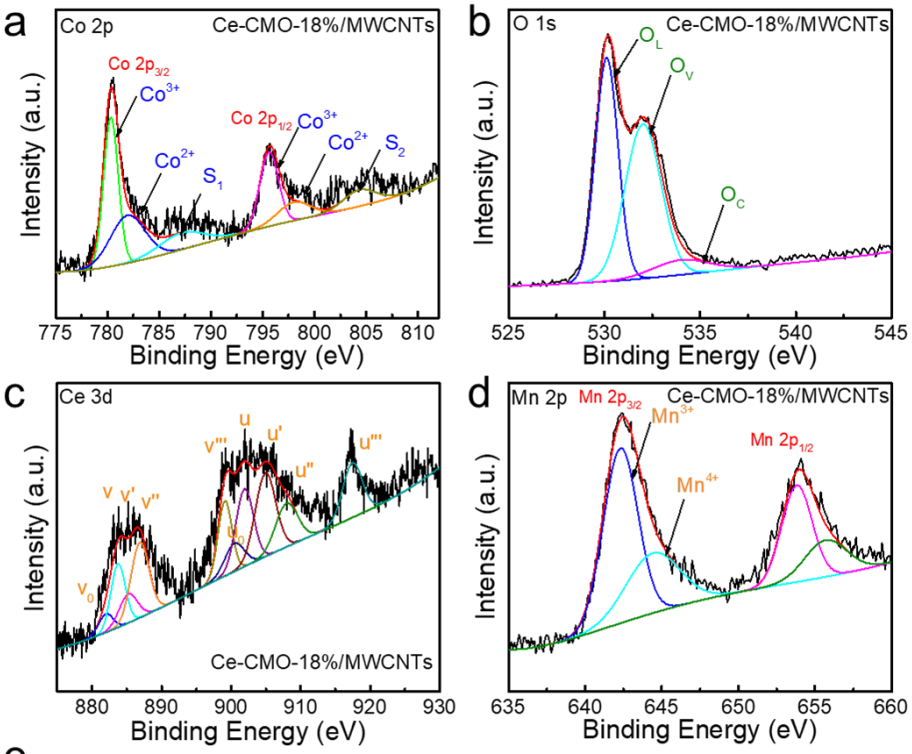


e

| Sample | Co 2p ($Co^{3+}/Co^{2+}$) | O 1s ($O_V/O_L$) | Ce 3d ($Ce^{3+}/Ce^{4+}$) | Mn 2p ($Mn^{4+}/Mn^{3+}$) |
|---|---|---|---|---|
| Ce-CMO-18% | 0.96 | 0.85 | 0.56 | 0.54 |
| Ce-CMO-18%/MWCNTs | 1.01 | 1.10 | 0.45 | 0.53 |

**Figure S12.** The XPS spectra of Ce-CMO-18%/MWCNTs: (a) Co 2p, (b) O 1s, (c) Ce 3d, and (d) Mn 2p; (e) The different ratio of elements surface chemical valence between Ce-CMO-18% and Ce-CMO-18%/MWCNTs.

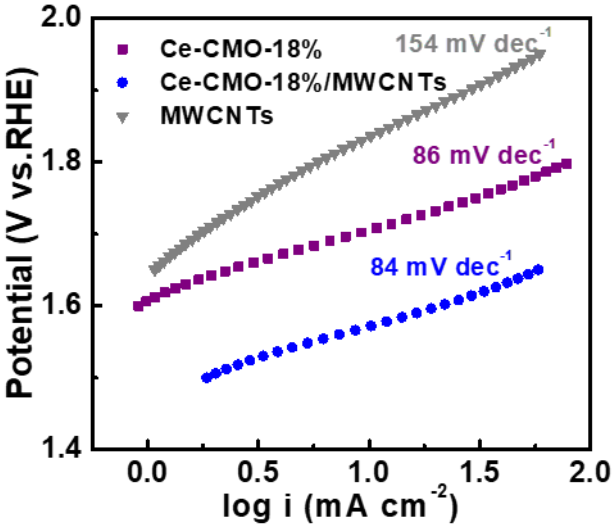


**Figure S13.** The corresponding Tafel plots of Ce-CMO-18%, Ce-CMO-18%/MWCNTs, and MWCNTs.

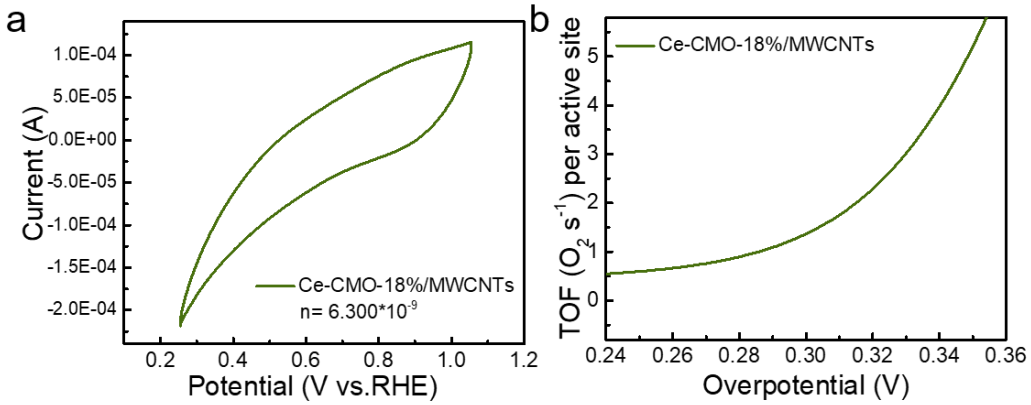


**Figure S14.** (a) CV curves of Ce-CMO-18%/MWCNTs in PBS solution (pH=7.0) at a scan rate of 50 mV $s^{-1}$, (b) Calculated $O_2$ TOF values of Ce-CMO-18%/MWCNTs.

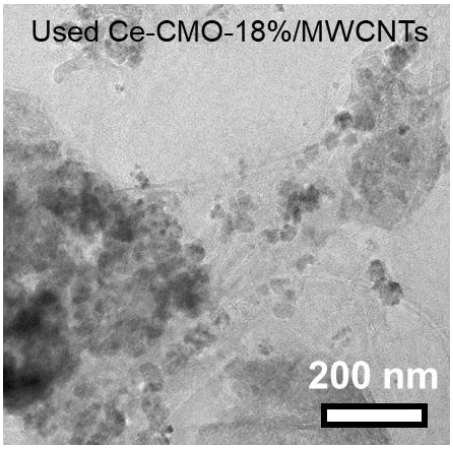


**Figure S15.** TEM image of the Ce-CMO-18%/MWCNTs after OER durability test.

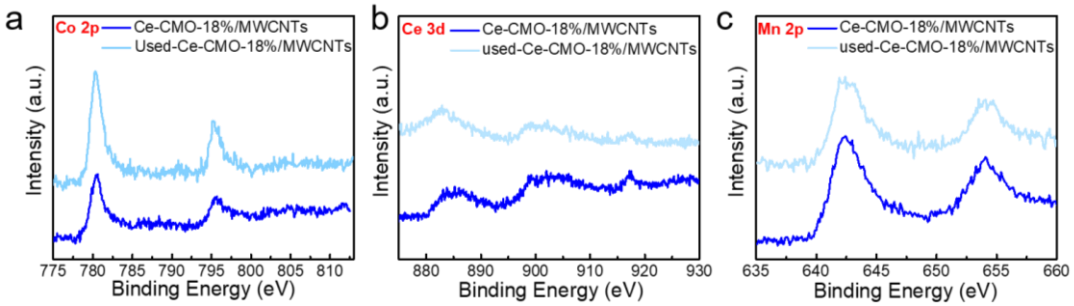


**Figure S16.** XPS spectra of the Ce-CMO-18%/MWCNTs before and after OER durability test: (a) Co 2p; (b) Ce 3d; (c) Mn 2p.

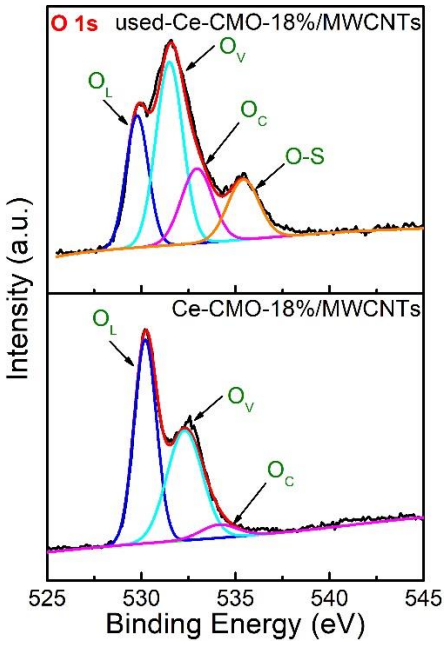


**Figure S17.** O 1s XPS spectra of the Ce-CMO-18%/MWCNTs before and after OER durability test.

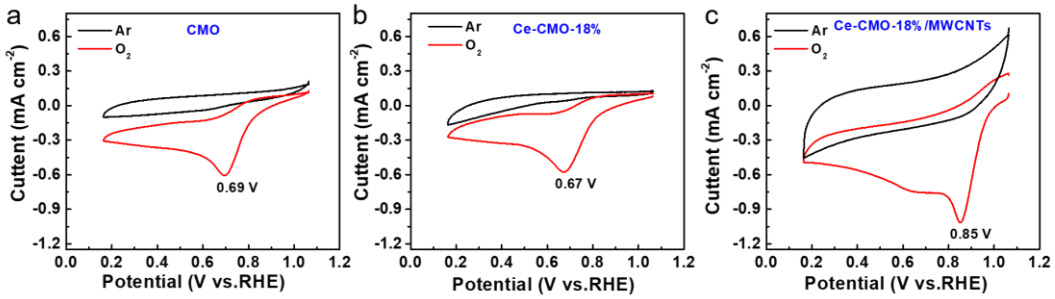


**Figure S18.** The cyclic voltammograms curves of (a) CMO, (b) Ce-CMO-18%, and (c) Ce-CMO-18%/MWCNTs in Ar- and $O_2$-saturated 1 M KOH aqueous solution.

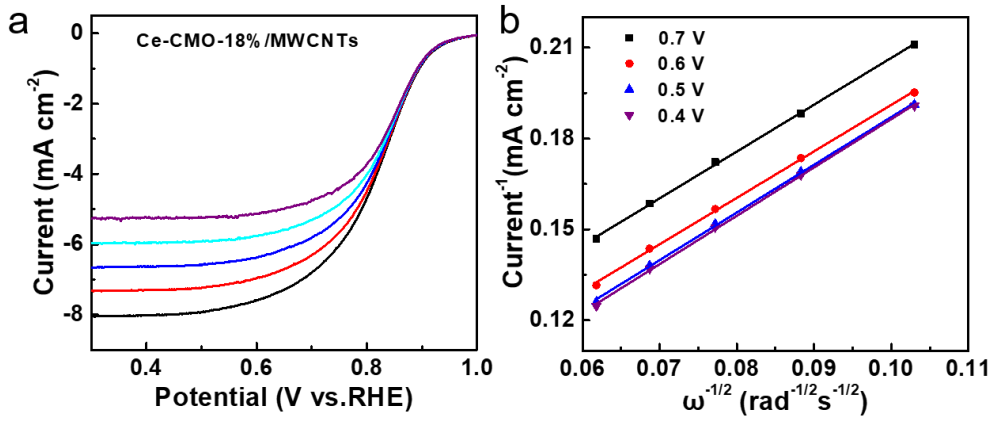


**Figure S19.** (a) Oxygen reduction polarization curves for Ce-CMO-18%/MWCNTs at 0.1 M KOH at various rotations rates; (b) Koutecky-Levich plots at different potentials (0.4, 0.5, 0.6, and 0.7 V *vs.* RHE) at a scan rate of 10 mV $s^{-1}$.

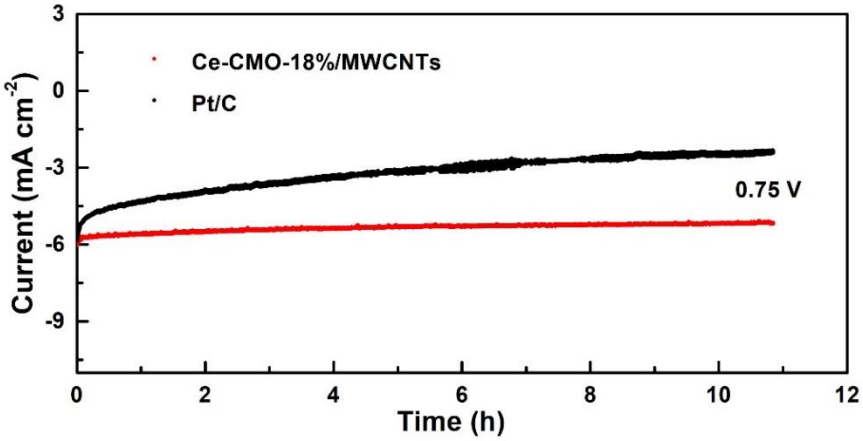


**Figure S20.** The chronoamperometry responses obtained on Pt/C and Ce-CMO-18%/MWCNTs at potential of 0.75 V.

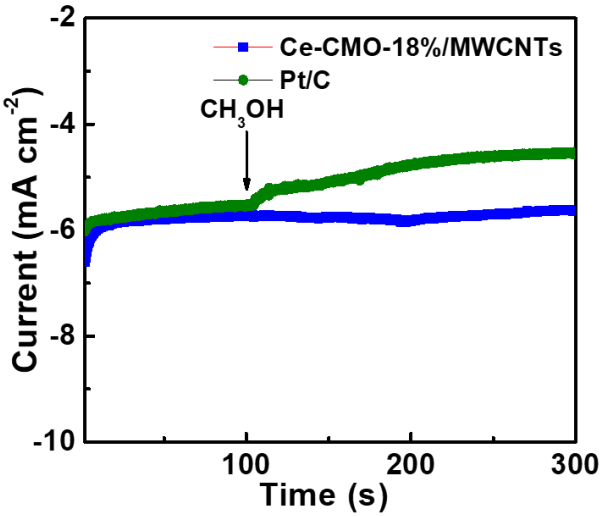


**Figure S21.** Current-time chronoamperometric response for Pt/C and Ce-CMO-18%/MWCNTs in $O_2$-saturated 0.1 M KOH with addition of methanol at 100 s.

**Turnover frequency (TOF) calculations:**

The calculation of TOF was referred from a method reported by Chang et. al [1] and Wang et. al [2] Typically, CV curves were recorded at a scan rate of 50 mV $s^{-1}$ in PBS solution (pH=7.0) as shown in Figure S10 and Figure S14. Then, the absolute value of the voltametric charges (anodic and cathodic) was evaluated by integrating the area under the curve. The quantity of active species (n) is calculated according to Equation S1.

$$n = \frac{Q}{2F} = \frac{It}{2F} = \frac{IV}{2Fv} \qquad \text{(S1)}$$

Where $Q$ is the voltametric charge, $F$ is Faraday constant (C $mol^{-1}$), $I$ is the current (A), $t$ is the time (s), $V$ is the voltage (V) and $v$ is the scanning rate (V $s^{-1}$).

The active site number of CMO, Ce-CMO-14%, Ce-CMO-18%, Ce-CMO-22%, and Ce-CMO-18%/MWCNTs are calculated to be $4.038 \times 10^{-9}$, $4.500 \times 10^{-9}$, $5.364 \times 10^{-9}$, $4.548 \times 10^{-9}$, and $6.300 \times 10^{-9}$ mol, respectively. After that, the TOF can be calculated by Equation S2:

$$TOF = \frac{|j|\,A}{nmF} \qquad \text{(S2)}$$

Where $j$ is the current (A) during the LSV tests, $A$ is the area of the electrode (1 cm-1), $n$ is the number of active sites (mol), and $m$ is the number of electrons transferred to generate one molecule of the product ($m$=4 for OER).

**References:**

[1] Chang, K., Tran, D. T., Wang, J. Q., Kim, N. H., Lee, J. H. A 3D hierarchical network derived from 2D Fe-doped NiSe nanosheets/carbon nanotubes with enhanced OER performance for overall water splitting. *J. Mater. Chem. A* **2022**, *10*, 3102-3111.

[2] Singh. T. I., Maibam, A., Cha, D. C., Yoo, S., Babarao, R., Lee, S. U., Lee, S. High-alkaline water-splitting activity of mesoporous 3D heterostructures: an amorphous-shell@crystalline-core nano-assembly of Co-Ni-Phosphate ultrathin-nanosheets and V- doped Cobalt-Nitride nanowires. *Adv. Sci.* **2022**, *9*, 2201311.